

# Application for Superconvergence of Finite Element Approximations for the Elliptic Problem by Global and Local $L^2$ -Projection Methods

Rabeea H. Jari, Lin Mu

Department of Applied Science, UALR, Little Rock, USA  
 Email: rhjari@ualr.edu, lxmu@ualr.edu

Received February 12, 2012; revised May 21, 2012; accepted July 12, 2012

## ABSTRACT

Numerical experiments are given to verify the theoretical results for superconvergence of the elliptic problem by global and local  $L^2$ -Projection methods.

**Keywords:** Finite Element Methods; Superconvergence;  $L^2$ -Projection; Elliptic Problem

## 1. Introduction

The elliptic problem seeks  $u$  in a certain functional space such that

$$-\Delta u = f \text{ in } \Omega \quad (1)$$

$$u = g \text{ in } \partial\Omega \quad (2)$$

where  $\Delta$  denote the Laplacian operator.

Let  $T_h$  be a finite element partition of the domain  $\Omega$  with characteristic mesh size  $h$ . Let  $V_h \subset H_g^1(\Omega)$  be any finite element space for  $u$  associated with the partition  $T_h$ .

The  $L^2$ -Projection technique was introduced by Wang [1-3]. It projects the approximate solution to another finite element dimensional space associated with a coarse mesh.

Now, we start with defining a coarse mesh  $T_\tau$  where  $\tau \gg h$  satisfying:

$$\tau = h^\alpha \quad (3)$$

with  $\alpha \in (0,1)$ . Define finite element space  $V_\tau \subset H^{s-2}(\Omega)$ . Let  $Q_\tau$  to be the  $L^2$ -Projector onto the finite element space  $V_\tau$  [1,4,5]. The Projector  $Q_\tau$  can be considered as a linear operator (projection) from  $L^2(\Omega)$  onto the finite element space  $V_\tau$  [6,7].

## 2. Superconvergence by Global $L^2$ -Projection

The following theorems can be found in [1].

**Theorem 2.1:** Assume that  $1 \leq s \leq k+1$  and the finite element space  $V_\tau \subset H^{s-2}(\Omega)$ . If the exact solution  $u \in H^{k+1}(\Omega) \cap H^{r+1}(\Omega) \cap H_g^1(\Omega)$ , then there exists a

constant  $C$  such that

$$\begin{aligned} & \|u - Q_\tau u_h\| + h^\alpha \|\nabla_\tau(u - Q_\tau u_h)\| \\ & \leq Ch^{\alpha(r+1)} \|u\| + Ch^\sigma \|\nabla(u - u_h)\|, \end{aligned}$$

where  $\sigma = s - 1 + \alpha \min(0, 2 - s)$  and  $u_h$  is the finite element approximation of (1)-(2).

**Theorem 2.2:** Suppose that  $1 \leq s \leq k+1$ . Let the surface fitting spaces  $V_\tau \subset H^{s-2}(\Omega)$  and  $u_h$  be the finite element approximation of (1)-(2). Then, the post-processing of  $u_h$  is estimated by

$$\alpha = \frac{k + s - 1}{r + 1 - \min(0, 2 - s)}.$$

## 3. Numerical Experiments for Global $L^2$ -Projection

In this section, we present several numerical experiments to verify the theoretical analysis in [1]. The triangulation  $T_h$  is constructed by: 1) dividing the domain into an  $n^3 \times n^3$  rectangular mesh; 2) connecting the diagonal line with the positive slope. Denote  $h = \frac{1}{n^3}$  as the mesh size.

The finite element space is defined by

$$V_h = \{v \in H_g^1(\Omega); v|_K \in P_1(K); \forall K \in T_h, v = g \text{ on } \partial\Omega\}.$$

We define  $V_\tau$  as follows:

$$V_\tau = \{v \in L^2(\Omega); v|_K \in P_2(K); \forall K \in T_\tau\}.$$

**Example 3.1:** Let the domain  $\Omega = [0,1] \times [0,1]$  and the exact solution is assumed as

$$u = x(1-x)y(1-y)$$

**Table 1** shows that after the post-processing method, all the errors are reduced. The exact solution in  $L^2$ -norm of  $\|u - Q_\tau u_h\|$  has the similar convergence rate as  $\|u - u_h\|$ . There is no improvement for the  $u$  in  $L^2$ -norm. However, the error in  $H^1$ -norm have higher convergence rate, which is shown as  $O(h^{1.3})$  for  $\|\nabla_\tau(u - Q_\tau u_h)\|$ .

The order of convergence rate is  $O(h^{0.3})$  better than  $\|\nabla(u - u_h)\|$ , see **Figures 1(a)** and **(b)**.

**Figures 2(a)** and **(b)** give results for the finite element approximation of (1)-(2) before and after post-processing.

**Example 3.2:** Let the domain  $\Omega = [0,1] \times [0,1]$  and the exact solution is assumed as

$$u = \sin(\pi x) \cos(\pi y)$$

**Table 1. Errors on uniform triangular meshes  $T_h$  and  $T_\tau$ .**

$h$	$ u - u_h _1$	$\ u - u_h\ $	$ u - Q_\tau u_h _1$	$\ u - Q_\tau u_h\ $
$2^{-3}$	0.6632e-2	0.1287e-3	0.1427e-2	0.1227e-3
$3^{-3}$	0.2799e-2	0.2295e-4	0.4332e-3	0.2185e-4
$4^{-3}$	0.1433e-2	0.6017e-5	0.1763e-3	0.5730e-5
$5^{-3}$	0.8294e-3	0.2015e-5	0.8504e-4	0.1919e-5
$6^{-3}$	0.5223e-3	0.7992e-6	0.4596e-4	0.7610e-6
$O(h)$	0.9998	1.9993	1.3504	1.9996

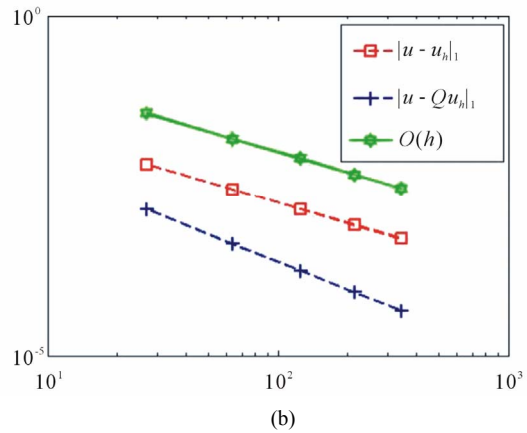
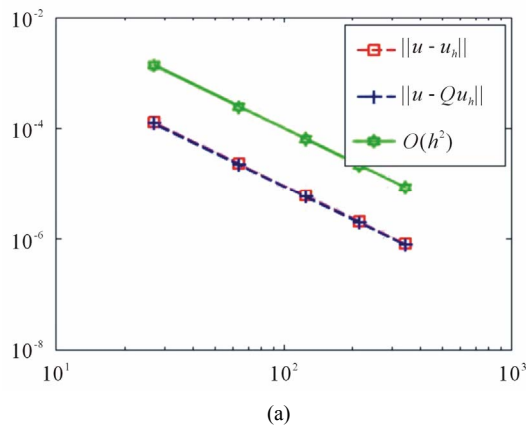


**Figure 1. (a) Convergence rate of  $L^2$ -norm error; (b) Convergence rate of  $H^1$ -norm error.**

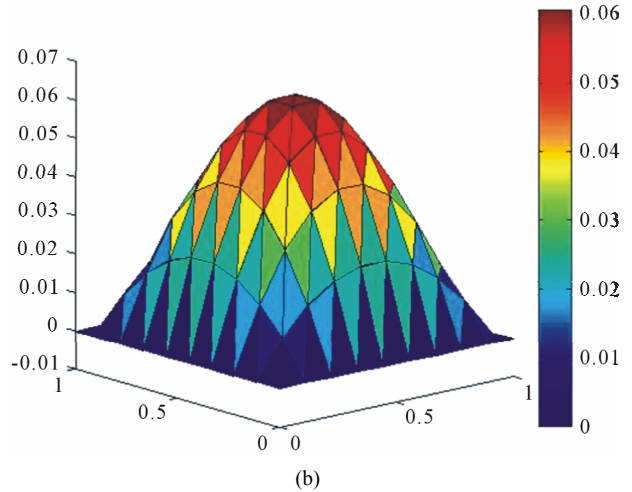
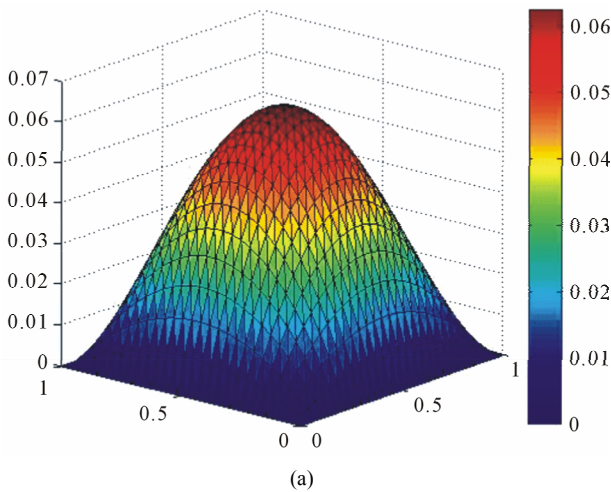


**Figure 2. (a) Surface plot of approximation solution  $u_h$ ; (b) Surface plot of approximation solution  $Q_\tau u_h$ .**

From the results shown in **Table 2**, it is clear that the exact solution  $u$  in  $H^1$ -norm has the superconvergence, but there is no improvement in the  $L^2$ -norm, see **Figures 3(a)** and **(b)**. The finite element solution given in **Figures 4(a)** and **(b)**. This agrees well with the theory.

**Example 3.3:** Let the domain  $\Omega = [0,1] \times [0,1]$  and the exact solution is assumed as

$$u = \frac{\cos(\pi(x+y))}{2}$$

**Table 3** gives the errors profile for Example 3. Notice that, the gradient estimate is of order  $O(h^{1.3})$ , that is much better than the optimal order  $O(h)$ . Although, there is no improvement in the  $L^2$ -norm, see **Figure 5**.

**Figure 6** shows that the approximation solutions  $u_h$  and  $Q_\tau u_h$ .

Also, our numerical results and theoretical conclusions in Theorems (2.1)-(2.2) show highly consistent.

**Table 2. Errors on uniform triangular meshes  $T_h$  and  $T_\tau$ .**

$h$	$ u - u_h _1$	$\ u - u_h\ $	$ u - Q_\tau u_h _1$	$\ u - Q_\tau u_h\ $
$2^{-3}$	0.9629e-1	0.1598e-2	0.2242e-1	0.1498e-2
$3^{-3}$	0.4063e-1	0.2850e-3	0.6872e-2	0.2669e-3
$4^{-3}$	0.2080e-1	0.7475e-4	0.2810e-2	0.6998e-4
$5^{-3}$	0.1204e-1	0.2503e-4	0.1359e-2	0.2343e-4
$6^{-3}$	0.7582e-2	0.9929e-5	0.7363e-3	0.9294e-5
$O(h)$	0.9998	1.9991	1.3427	1.9995

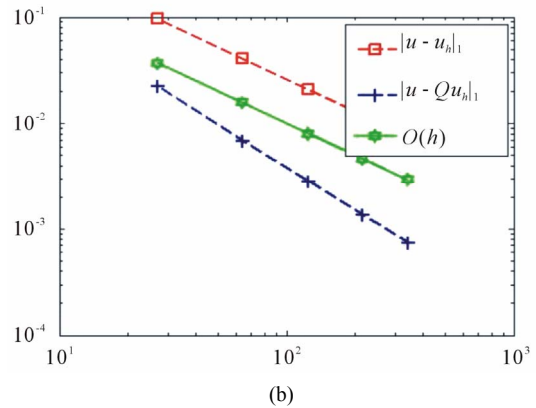
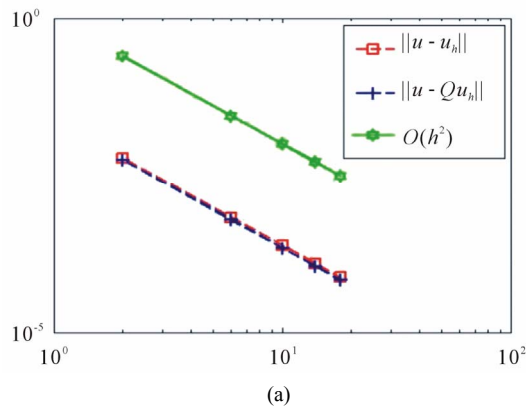


**Figure 3. (a) Convergence rate of error  $L^2$ -norm error; (b) Convergence rate of  $H^1$ -norm error.**

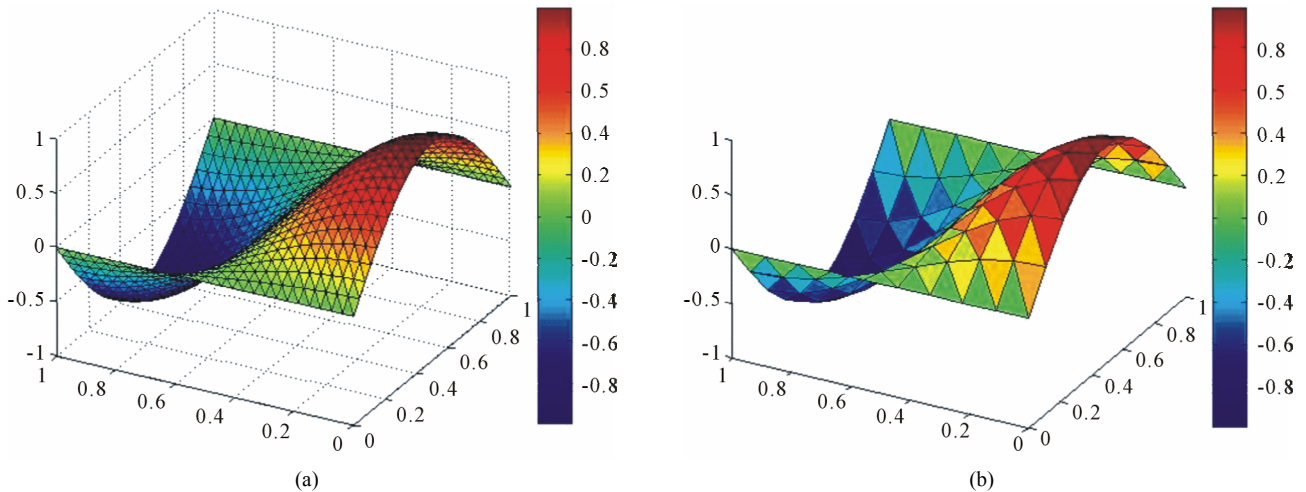


**Figure 4. (a) Surface plot of solution  $u_h$ ; (b) Surface plot of approximation solution  $Q_\tau u_h$ .**

**Table 3. Errors on uniform triangular meshes  $T_h$  and  $T_\tau$ .**

$h$	$ u - u_h _1$	$\ u - u_h\ $	$ u - Q_h u_h _1$	$\ u - Q_h u_h\ $
$2^{-3}$	0.9135e-1	0.1770e-2	0.2150e-1	0.1689e-2
$3^{-3}$	0.3855e-1	0.3157e-3	0.6579e-2	0.3010e-3
$4^{-3}$	0.1973e-1	0.8278e-4	0.2692e-2	0.7893e-4
$5^{-3}$	0.1142e-1	0.2772e-4	0.1303e-2	0.2643e-4
$6^{-3}$	0.7193e-2	0.1099e-4	0.7062e-3	0.1048e-4
$O(h)$	0.9999	1.9993	1.3424	1.9994

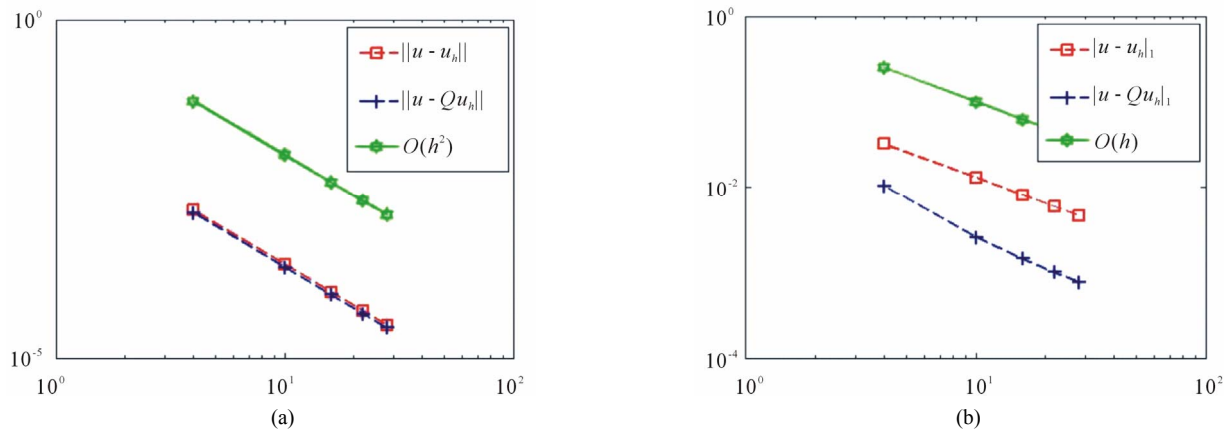


**Figure 5. (a) Convergence rate of  $L^2$ -norm error; (b) Convergence rate of  $H^1$ -norm error.**

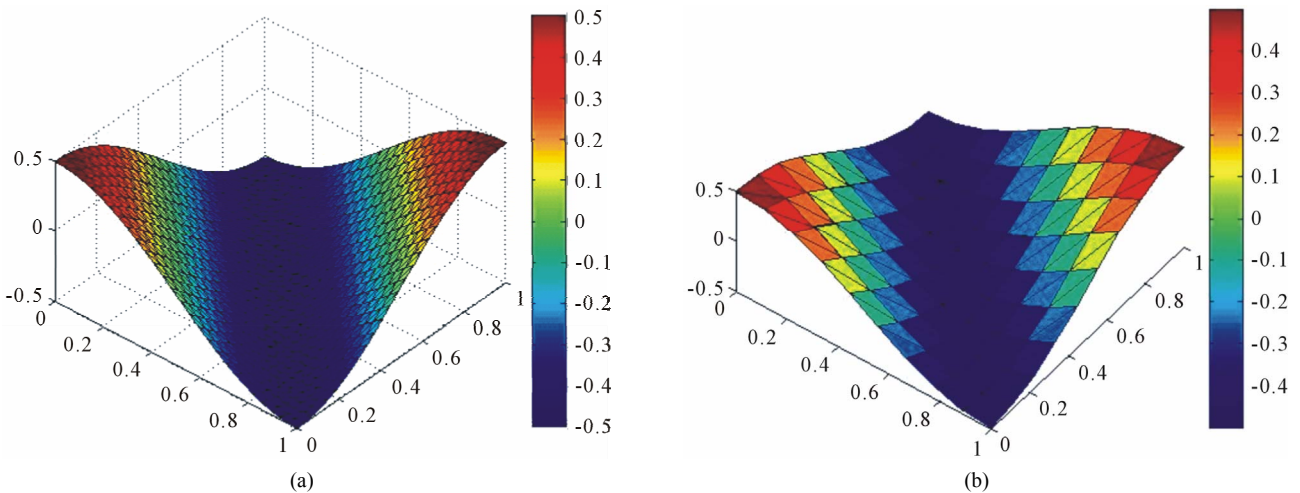


**Figure 6. (a) Surface plot of approximation solution  $u_h$ ; (b) Surface plot of approximation solution  $Q_\tau u_h$ .**

### 4. Superconvergence by Local $L^2$ -Projection

Notice that, the exact solution  $u$  may be not smooth globally on  $\Omega$  in practical computation, although the solution might be smooth enough locally for a good super convergence.

To this end, let  $\Omega_0$  be a subdomain of  $\Omega$  where the exact solution  $u$  is sufficiently smooth. Let  $\Omega_1$  be an-

other subdomain of  $\Omega$  such that  $\Omega_0 \subset \Omega_1$ . Define finite element space  $V_\tau \subset H^{s-2}(\Omega_1)$ . The  $L^2$ -projection  $Q_\tau$  from  $L^2(\Omega)$  onto the finite element space  $V_\tau$  is said to be local  $L^2$ -projection.

The following theorem can be found in [1].

**Theorem 4.1:** Assume that  $1 \leq s \leq k+1$  and the finite element space  $V_\tau \subset H^{s-2}(\Omega_0)$ . If the exact solution  $u \in H^{k+1}(\Omega) \cap H^{r+1}(\Omega_0) \cap H_g^1(\Omega)$ , then there exists a

constant  $C$  such that

$$\begin{aligned} & \|u - Q_\tau u_h\|_{\Omega_0} + h^\alpha \|\nabla_\tau (u - Q_\tau u_h)\|_{\Omega_0} \\ & \leq Ch^{\alpha(r+1)} \|u\|_{\Omega_0} + Ch^\alpha \|\nabla(u - u_h)\|_{\Omega_0}, \end{aligned}$$

where  $u_h$  is the finite element approximation of (1)-(2).

**Theorem 4.2:** Suppose that  $1 \leq s \leq k + 1$ . Let the surface fitting spaces  $V_\tau \subset H^{s-2}(\Omega_0)$  and  $u_h$  be the finite element approximation of (1)-(2). Then, the post-processing of  $u_h$  is estimated by

$$\alpha = \frac{k + s - 1}{r + 1 - \min(0, 2 - s)}$$

### 5. Numerical Experiments for Local $L^2$ -Projection

In this section, we present several numerical experiments to verify the theoretical analysis in [1]. The triangulation  $T_h$  is constructed by: 1) dividing the domain into an  $n^3 \times n^3$  rectangular mesh; 2) connecting the diagonal line with the positive slope. Denote  $h = \frac{1}{n^3}$  as the mesh size.

The finite element space is defined by

$$V_h = \{v \in H^1_g(\Omega); v|_K \in P_1(K); \forall K \in T_h, v = g \text{ on } \partial\Omega\}.$$

We define  $V_\tau$  as follows:

$$V_\tau = \{v \in L^2(\Omega); v|_K \in P_2(K); \forall K \in T_\tau\}.$$

**Example 5.1:** Let the domain  $\Omega = [0,1] \times [0,1]$  and  $\Omega_0 = [0, 0.5] \times [0, 0.5]$ . The exact solution is assumed as

$$u = \frac{1}{2 - x - y}$$

It is clear that the exact solution  $u$  is singular and  $f$  blows down at the boundary of  $\Omega = [0,1] \times [0,1]$ , see

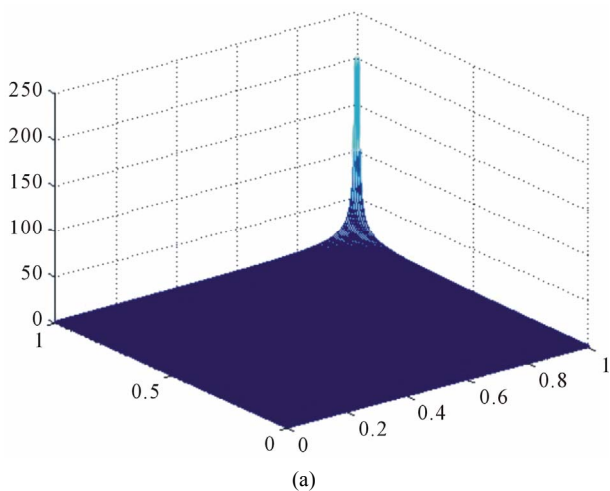


**Figure 7**, however,  $u_h$  and  $Q_\tau u_h$  are sufficiently smooth on  $\Omega = [0,1] \times [0,1]$ , see **Figure 8**.

**Table 4** shows that after the post-processing method, all the errors are reduced. The exact solution in  $L^2$ -norm of  $\|u - Q_\tau u_h\|$  has the similar convergence rate as  $\|u - u_h\|$  which is shown as  $O(h^2)$ . There is no improvement for the  $u$  in  $L^2$ -norm. However, the error in  $H^1$ -norm have higher convergence rate, which is shown as  $O(h^{1.3})$  for  $\|\nabla_\tau (u - Q_\tau u_h)\|$ . The order of convergence rate is  $O(h^{0.3})$  better than  $\|\nabla_h(u - u_h)\|$ , see **Figure 9**.

**Example 5.2:** Let the domain  $\Omega = [0,1] \times [0,1]$  and  $\Omega_0 = [0.5,1] \times [0.5,1]$ . The exact solution is assumed as

$$u = \sqrt{x^2 + y^2}$$

Obviously, the exact solution has singularity on the origin at the domain  $\Omega = [0,1] \times [0,1]$ , see **Figure 10(a)**. On the same domain the function  $f$  blows down at the boundary, see **Figure 10(b)**. The approximation solutions  $u$  and  $Q_\tau u_h$  have been plot in the proper subdomain  $\Omega_0 = [0.5,1] \times [0.5,1]$ , see **Figure 11**.

From the results shown in **Table 5**, it is clear that the exact  $u$  in  $H^1$ -norm has the superconvergence, but there is no improvement in the  $L^2$ -norm, see **Figure 12**. This agrees well with the theory.

**Example 6:** Let the domain  $\Omega = [0,1] \times [0,1]$  and  $\Omega_0 = [0.5,1] \times [0.5,1]$ . The exact solution is assumed as

$$u = \frac{y}{\sqrt{x^2 + y^2}}$$

From **Figures 13(a)** and **(b)**, respectively observe that the exact solution has strongly singularity on the origin of the domain  $\Omega = [0,1] \times [0,1]$  and the function  $f$  blows up at the boundary, **Figure 14** show how the approximation solution  $u_h$  and  $Q_\tau u_h$  look like at the proper subdomain  $\Omega_0 = [0.5,1] \times [0.5,1]$ .

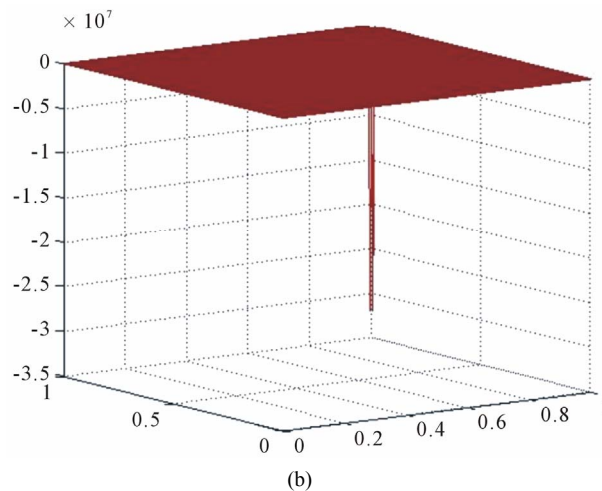


**Figure 7.** (a) The exact solution  $u$  blows up; (b)  $f$  blows down at the boundary.



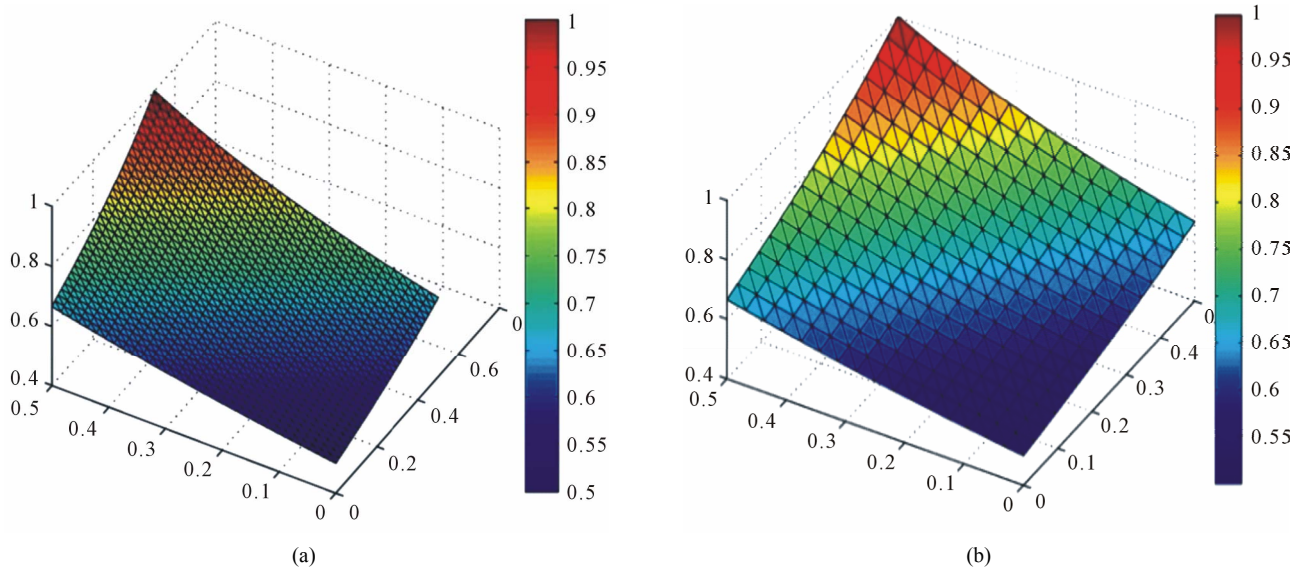


Figure 8. (a) Surface plot of approximation solution  $u_h$ ; (b) Surface plot of approximation solution  $Q_\tau u_h$ .

Table 4. Errors on uniform triangular meshes  $T_h$  and  $T_\tau$ .

$h$	$ u - u_h _1$	$\ u - u_h\ $	$ u - Q_\tau u_h _1$	$\ u - Q_\tau u_h\ $
$2^{-3}$	0.3221e-1	0.1497e-2	0.1026e-1	0.1363e-2
$3^{-3}$	0.1291e-1	0.2384e-3	0.2566e-2	0.2169e-3
$4^{-3}$	0.8072e-2	0.9306e-4	0.1429e-2	0.8466e-4
$5^{-3}$	0.5871e-2	0.4921e-4	0.9977e-3	0.4476e-4
$6^{-3}$	0.4613e-2	0.3037e-4	0.7691e-3	0.2763e-4
$O(h)$	0.9998	2.0030	1.3360	2.0035

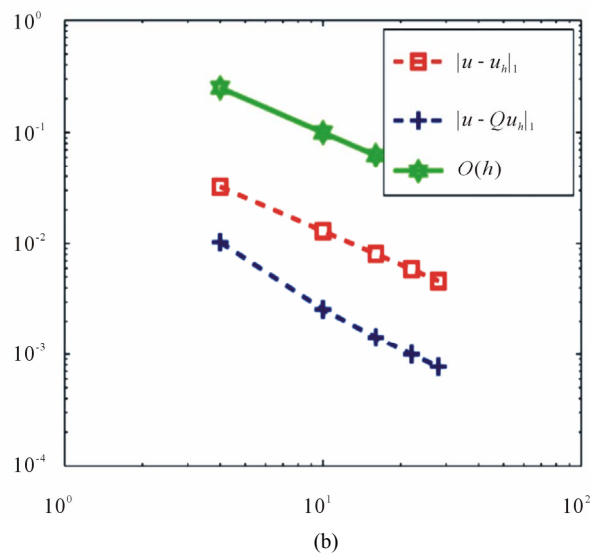
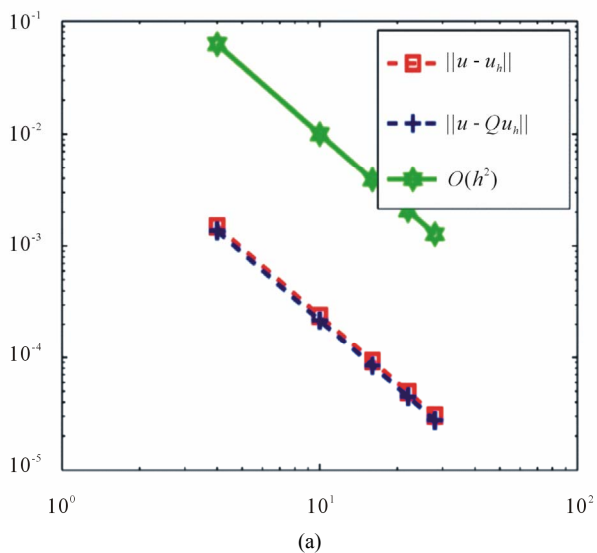


Figure 9. (a) Convergence rate of  $L^2$ -norm error; (b) Convergence rate of  $H^1$ -norm error.

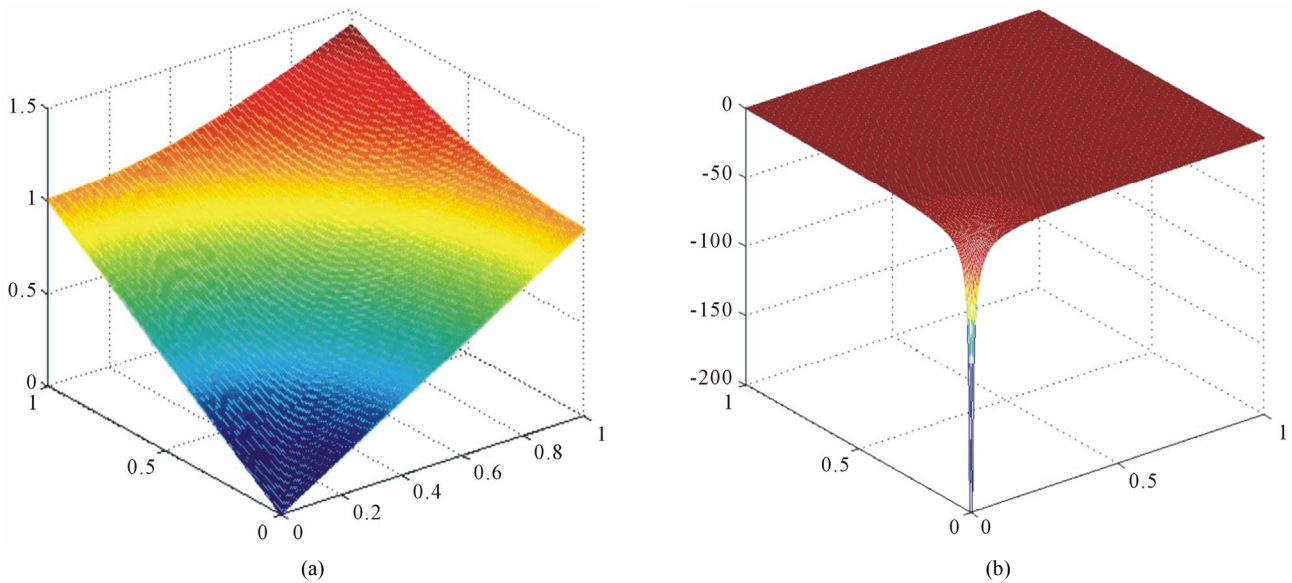


Figure 10. (a) Surface plot of exact solution  $u$ ; (b)  $f$  blows down at the boundary.

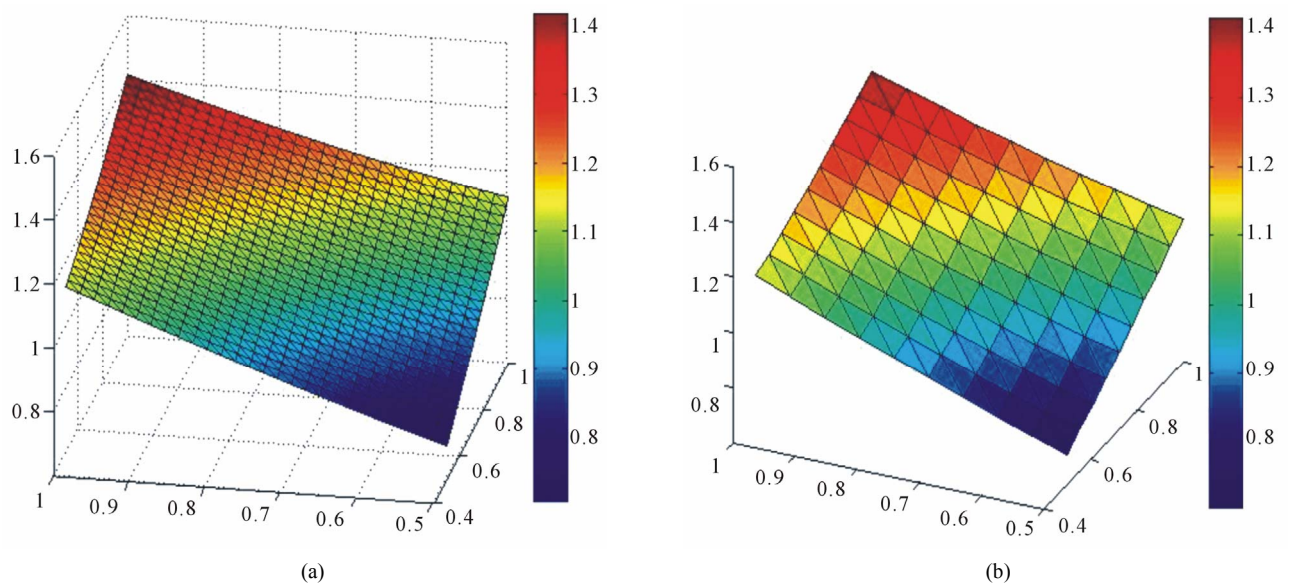


Figure 11. (a) Surface plot of approximation solution  $u_h$ ; (b) Surface plot of approximation solution  $Q_\tau u_h$ .

Table 5. Errors on uniform triangular meshes  $T_h$  and  $T_\tau$ .

$h$	$ u - u_h $	$\ u - u_h\ $	$ u - Q_\tau u_h $	$\ u - Q_\tau u_h\ $
$2^{-3}$	$0.1352e-1$	$0.1400e-2$	$0.6141e-2$	$0.1287e-2$
$3^{-3}$	$0.6835e-2$	$0.3596e-3$	$0.2110e-2$	$0.3314e-3$
$4^{-3}$	$0.4566e-2$	$0.1607e-3$	$0.1215e-2$	$0.1481e-3$
$5^{-3}$	$0.3427e-2$	$0.9058e-4$	$0.8529e-3$	$0.8352e-4$
$6^{-3}$	$0.2743e-2$	$0.5802e-4$	$0.6590e-3$	$0.5350e-4$
$O(h)$	0.9923	1.9806	1.3581	1.9792

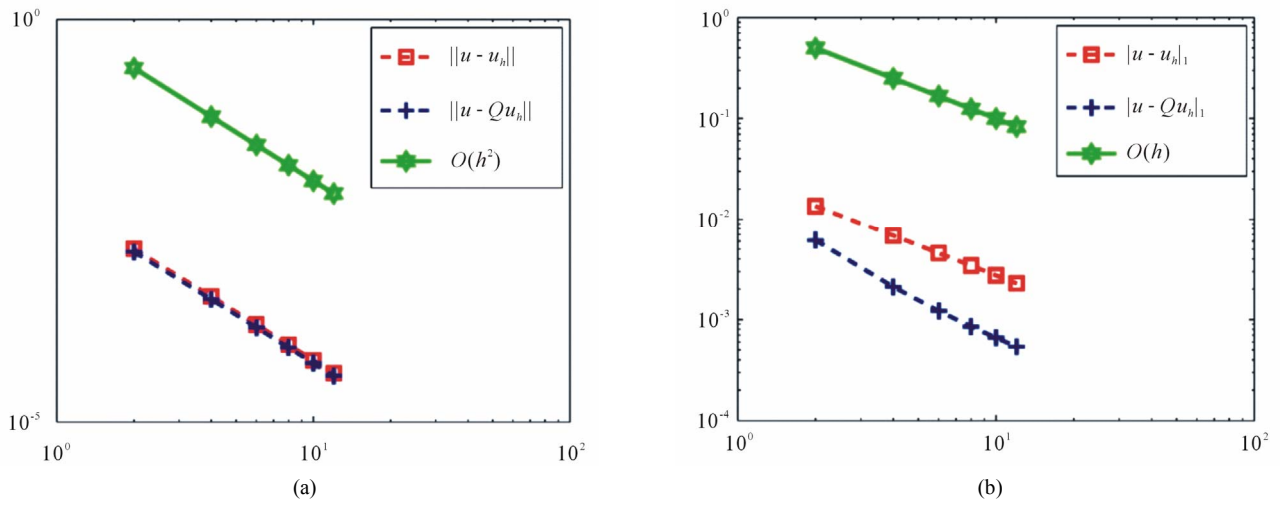


Figure 12. (a) Convergence rate of  $L^2$ -norm error; (b) Convergence rate of  $H^1$ -norm error.

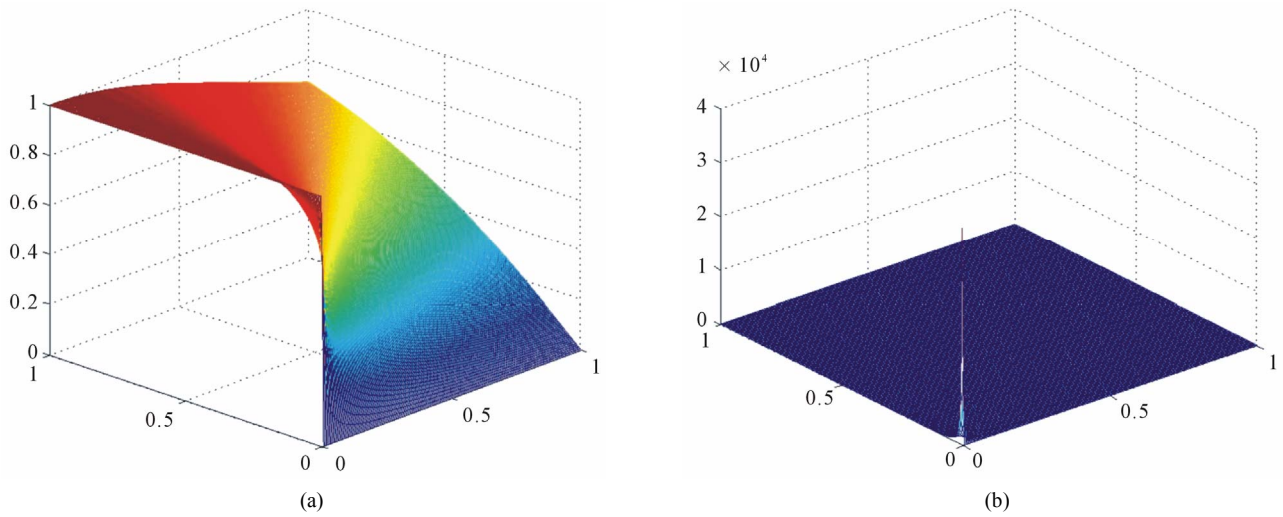


Figure 13. (a) Surface plot of exact solution  $u$ ; (b)  $f$  blows up at the boundary.

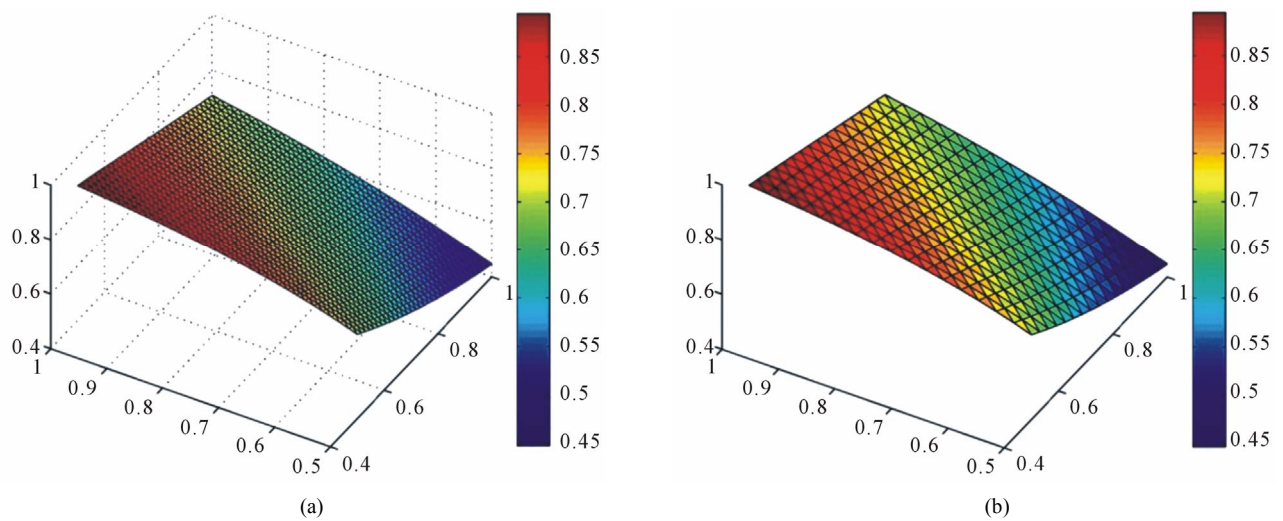
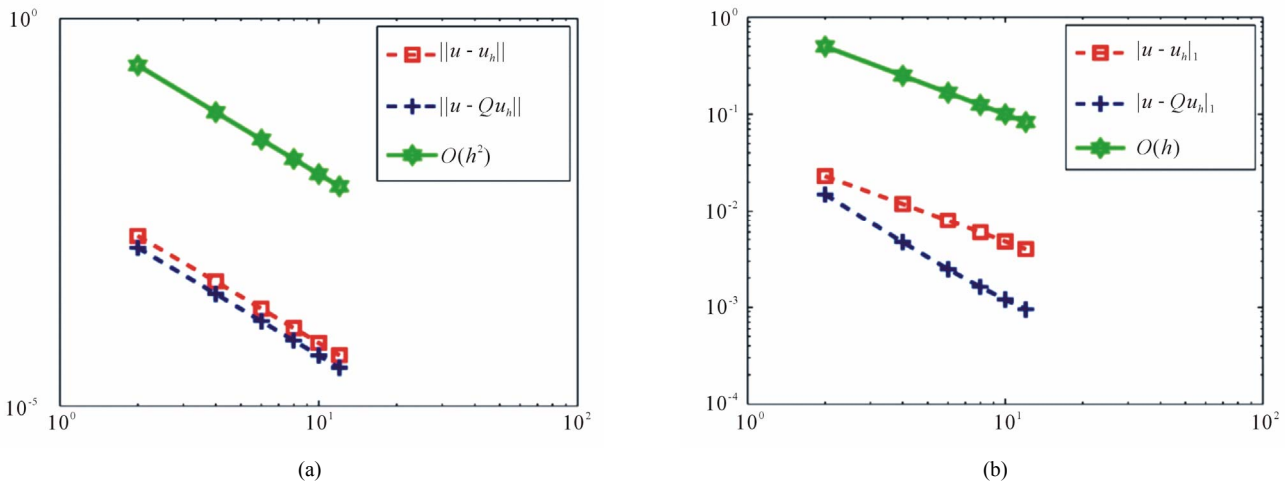


Figure 14. (a) Surface plot of approximation solution  $u_h$ ; (b) Surface plot of approximation solution  $Q_\tau u_h$ .



**Table 6. Errors on uniform triangular meshes  $T_h$  and  $T_\tau$ .**

$h$	$ u - u_h _1$	$\ u - u_h\ $	$ u - Qu_h _1$	$\ u - Qu_h\ $
$2^{-3}$	0.1186e-1	0.4006e-3	0.4708e-2	0.2779e-3
$3^{-3}$	0.5979e-2	0.1009e-3	0.1621e-2	0.6959e-4
$4^{-3}$	0.3992e-2	0.4490e-4	0.9518e-3	0.3094e-4
$5^{-3}$	0.2996e-2	0.2527e-4	0.6760e-3	0.1740e-4
$6^{-3}$	0.2397e-2	0.1617e-4	0.5261e-3	0.1113e-4
$O(h)$	0.9943	1.9949	1.3304	1.9989



**Figure 15. (a) Convergence rate of  $L^2$ -norm error; (b) Convergence rate of  $H^1$ -norm error.**

**Table 6** gives the errors profile for Example 6. Notice that, the gradient estimate is of order  $O(h^{1.3})$  that is much better than the optimal order  $O(h)$ . Although, there is no improvement in the  $L^2$ -norm, see **Figure 15**. Also, the numerical results and theoretical conclusions show highly consistent.

**REFERENCES**

[1] J. Wang, "A Superconvergence Analysis for Finite Element Solutions by the Least-Squares Surface Fitting on Irregular Meshes for Smooth Problems," *Journal of Mathematical Study*, Vol. 33, No. 3, 2000, pp. 229-243.

[2] R. E. Ewing, R. Lazarov and J. Wang, "Superconvergence of the Velocity along the Gauss Lines in Mixed Finite Element Methods," *SIAM Journal on Numerical Analysis*, Vol. 28, No. 4, 1991, pp. 1015-1029. [doi:10.1137/0728054](https://doi.org/10.1137/0728054)

[3] M. Zlamal, "Superconvergence and Reduced Integration

in the Finite Element Method," *Mathematics Computation*, Vol. 32, No. 143, 1977, pp. 663-685. [doi:10.2307/2006479](https://doi.org/10.2307/2006479)

[4] L. B. Wahlbin, "Superconvergence in Galerkin Finite Element Methods," Lecture Notes in Mathematics, Springer, Berlin, 1995.

[5] A. H. Schatz, I. H. Sloan and L. B. Wahlbin, "Superconvergence in Finite Element Methods and Meshes that Are Symmetric with Respect to a Point," *SIAM Journal on Numerical Analysis*, Vol. 33, No. 2, 1996, pp. 505-521. [doi:10.1137/0733027](https://doi.org/10.1137/0733027)

[6] M. Krizaek and P. Neittaanmaki, "Superconvergence Phenomenon in the Finite Element Method Arising from Averaging Gradients," *Numerische Mathematik*, Vol. 45, No. 1, 1984, pp. 105-116.

[7] J. Douglas and T. Dupont, "Superconvergence for Galerkin Methods for the Two-Point Boundary Problem via Local Projections," *Numerical Mathematics*, Vol. 21, No. 3, 1973, pp. 270-278. [doi:10.1007/BF01436631](https://doi.org/10.1007/BF01436631)